Relating Hygroscopic Properties of Magnesium Nitrate to the Formation of Contact Ion Pairs

Yun-Hong Zhang,[†] Man Yee Choi,[‡] and Chak K. Chan*[,‡]

Department of Chemistry, School of Science, Beijing Institute of Technology, Beijing 100081, China, and Department of Chemical Engineering, Hong Kong University of Science and Technology, Clear Water Bay, Kowloon, Hong Kong, China

Received: August 24, 2003; In Final Form: December 9, 2003

The formation of contact ion pairs in $Mg(NO_3)_2$ solutions and their effects on the hygroscopic properties of the solutions were studied using Raman spectroscopy of $Mg(NO_3)_2$ droplets levitated in an electrodynamic balance. Upon reduction in the ambient relative humidity (RH), $Mg(NO_3)_2$ droplets lose water but do not effloresce. The molar water-to-solute ratio (WSR) decreases exponentially with decreasing RH, but it decreases linearly with RH when it is less than 6. This transition of hygroscopicity at WSR = 6 coincides with an abrupt blue shift of the ν_1 band of NO_3^- from 1049 to 1055 cm^{-1} in the Raman spectra, which is due to nitrate ions entering into the primary solvation shell of Mg^{2+} ions to form direct contact ion pairs. As the WSR further decreases, a shoulder on the higher wavenumber side of the ν_1 band appears near 1060 cm^{-1} and the separation of ν_3 bands increases because of the formation of more complex contact ion pairs. Raman images of supersaturated droplets at WSR = 2.8 show structural heterogeneity not found in diluted droplets. Overall, the NO_3^- to Mg^{2+} ratio increases and the H_2O to Mg^{2+} ratio decreases as the surface of the droplet is approached. However, droplets at low concentration (WSR = 9.6) show a uniform distribution of monodentates.

Introduction

The hygroscopic properties of atmospheric aerosols have been the focus of many research studies because the water content of the aerosols affects virtually all physical and chemical properties, and in turn, the environmental and health effects of aerosol particles have been investigated. Experimental measurements of hygroscopicity include the use of gravimetric analysis of filter samples,[1] relative mass measurements of single particles levitated in an electrodynamic balance (EDB),[2−4] size distribution measurements in a tandem differential mobility analyzer,[5−7] and the observation of water peaks in the FTIR spectra of particles in an aerosol flow tube.[8−10] Although the measurements of water absorption are useful in understanding the hygroscopic nature of the aerosols under study, they do not provide information on the chemical interactions in aqueous solutions, which are the molecular basis for water absorption. In particular, the chemical interactions between ions and between water and ions in concentrated aqueous aerosols, especially near efflorescence, are expected to be very different from those in diluted aqueous aerosols.

Recently, we have used Raman spectroscopy to investigate the relationship between the solute−water interactions and the hygroscopicity of single levitated aqueous droplets of several metal sulfate compounds and $(NH_4)_2SO_4$ in an EDB.[11,12] We found that, at high concentrations, the chemical interactions between water molecules, sulfate ions, and the countercations are significant. The strong interactions between sulfate and metal cations lead to the formation of contact ion pairs, which hinder the mass transfer of water and affect the crystallization process in $MgSO_4$ and its mixtures with Na_2SO_4. More recently, we have studied the structure of water molecules in $NaClO_4$, $LiClO_4$, and $Mg(ClO_4)_2$ solutions from diluted concentrations to high supersaturations.[13] Raman spectra of water monomers in highly supersaturated droplets were observed.

Nitrate is a common anion of atmospheric interest. Compared with sulfate aerosols of the same cation, nitrate aerosols are often found to crystallize at much lower relative humidities or not to crystallize at all in well-controlled experiments. Under these highly supersaturated conditions with little water, the interactions between the cation and nitrate are very strong, facilitating the formation of direct contact ion pairs. It has been found that the $Mg(NO_3)_2$ droplets do not crystallize even at high supersaturation. In this paper, the formation of contact ion pairs in $Mg(NO_3)_2$ solutions and their effects on the hygroscopic properties of the solution are examined. In addition, we investigate the spatial distributions of the contact ion pairs by Raman images of droplets. Structural heterogeneity of the Raman images is found in the supersaturated droplets but not in the diluted droplets.

Experimental Methods

The experimental setup and procedures used in this study are identical to those used in our previous work.[11−13] An electrodynamic balance (EDB) was used to trap and levitate single $Mg(NO_3)_2$ droplets. By proper adjustments of the electric field strength, a charged particle can be held stationary. When

* To whom all correspondence should be addressed. E-mail: keckchan@ust.hk.
[†] Beijing Institute of Technology. E-mail: yhz@bit.edu.cn.
[‡] Hong Kong University of Science and Technology.

10.1021/jp036524d CCC: $27.50
Published on Web 02/14/2004

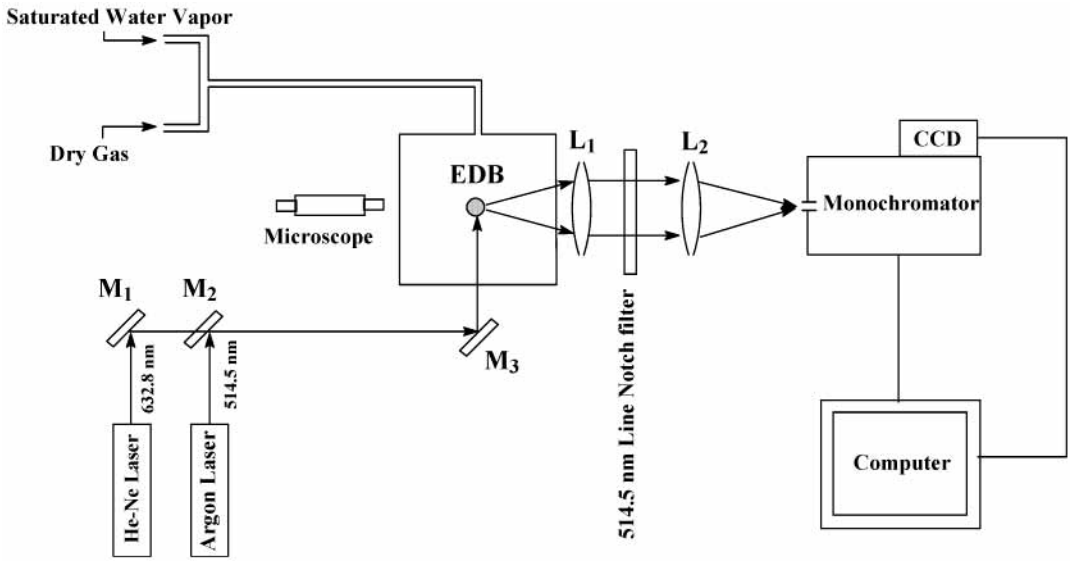

Figure 1. Experimental setup of single particle Raman spectroscopy.

exposed to a purified air stream of varying relative humidity, the particle will absorb an equilibrium amount of water. The equilibrium water content of the particle, in terms of the molar water-to-salt ratio (WSR) on a dry basis, is determined by measuring the applied voltage to balance a stationary particle.

The 514.5 nm line of an Ar^+ laser was used as the excitation light source. The nominal output power used was between 800 and 1000 mW in this study. A pair of lenses, matching the *f*/7 optics of the monochromator (Acton SpectraPro 500, Princeton Instruments, TE/CCD-1100PFUV)), was used to focus the 90° scattering of the levitated droplet to the slit of the monochromator. A 514.5 nm Raman notch-filter was placed between the two lenses to remove the strong Rayleigh scattering. The 300 g/m and 1200 g/mm gratings of the monochromator were selected to obtain the Raman spectra of the $Mg(NO_3)_2$ droplets for a wide spectral range (with a spectral resolution of about 10 cm^{-1}) and for a high spectral resolution (about 2.3 cm^{-1}), respectively. The spectra reported in this work were the averages of the 30 frames, each with an accumulation time of about 5 s. All measurements were made at ambient temperatures of 22−24 °C.

Figure 1 shows the experimental setup to measure the Raman scattering and the Raman image of a droplet. Because the droplet has a focus effect as a lens, there are two bright spots near at the top and the bottom of the droplet as a result of the irradiation of the laser. After focusing and the dispersion in the monochromator, the two-dimensional Raman signal received by the CCD detector provides a Raman image of the droplet. The horizontal pixels of the CCD detector represent the wavenumber and the vertical pixels represent the spatial (vertical) position of the droplet. Hence, a double crest Raman image showing maximum peak intensities at the top and bottom of a droplet was observed. Raman images were recorded with an accumulation time of 40−80 s. Binning of the vertical pixels was applied when the overall Raman scattering, but not the detailed image, was measured.

Results and Discussion

1. Hygroscopic Properties of $Mg(NO_3)_2$ Droplets. Figure 2 shows the hygroscopic properties of $Mg(NO_3)_2$ droplets in terms of the equilibrium molar WSR as a function of decreasing relative humidity (RH). Four particles were measured, and their

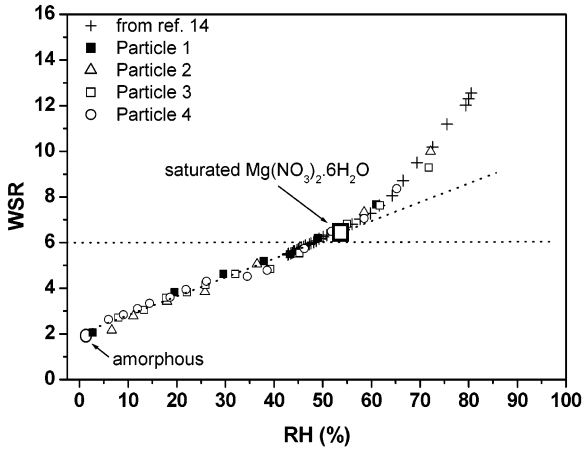

Figure 2. Hygroscopic properties of $Mg(NO_3)_2$ droplets.

results are consistent with those reported by Chan et al.,[14] who measured the WSR at RH higher than 40% only. We have extended the measurements to RH = 2.7%, corresponding to an extremely high supersaturation condition of WSR = 2.1, where one Mg^{2+} and two NO_3^- ions share only about two water molecules in the droplet on average. Overall, the WSR decreases exponentially with decreasing RH but a transition point exists at WSR = 6, below which the WSR decreases linearly with the RH. No efflorescence, which would result in a sudden decrease in the WSR, was observed in the evaporation experiments. However, an amorphous particle was occasionally formed with WSR = 2 without an efflorescence when the particle was exposed to dry gas (RH about 3%) for more than 10 h. Structural differences between a supersaturated droplet and the amorphous particle will be discussed below. Neither anhydrous $Mg(NO_3)_2$ nor the hexahydrate $Mg(NO_3)_2{\cdot}6H_2O$ was observed in our experiments.

2. Raman Spectra and the Formation of Contact Ion Pairs. Free NO_3^- has a plane structure with D_{3h} symmetry and has fundamental vibration bands at 1049, 830, ~1370, and 718 cm^{-1}, which correspond to the in-phase symmetric stretching mode ($\nu_1(A_1')$), the out-of-plane deformation mode ($\nu_2(A_2'')$), the out-of-phase stretching mode ($\nu_3(E')$), and the in-plane bending mode ($\nu_4(E')$), respectively. The ν_3 and ν_4 modes are both Raman and infrared active whereas the ν_1 mode is only Raman active and the ν_2 mode is only infrared active.[15−17]

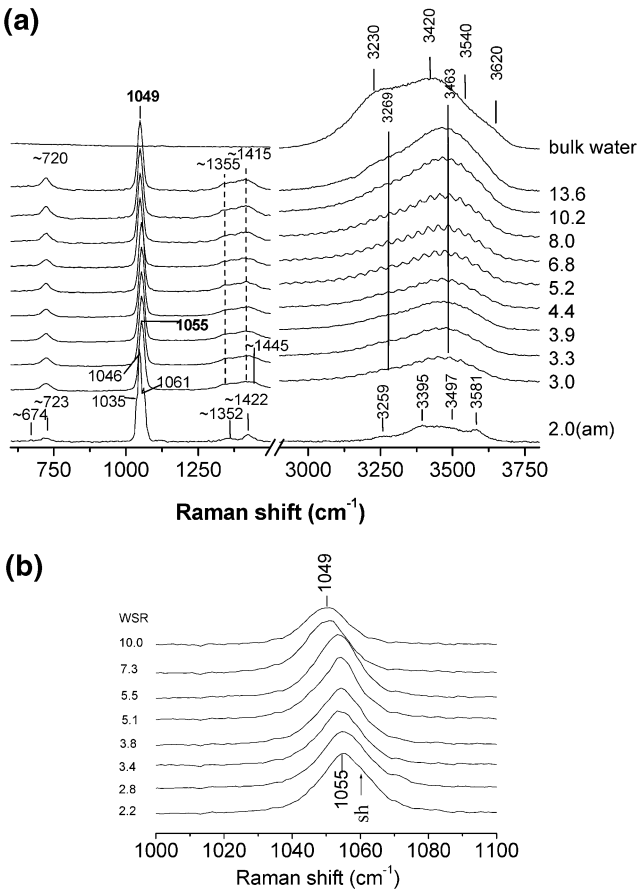

Figure 3. (a) Raman spectra $Mg(NO_3)_2$ droplets at various WSR (300 g/mm grating). (b) High-resolution Raman spectra of $Mg(NO_3)_2$ droplets (1200 g/mm grating).

However, even in diluted solutions, the Raman spectrum contains a pair of closely spaced lines (ν_{3a} and ν_{3b}) due to the hydration of nitrate, instead of the single ν_3 mode of the unperturbed nitrate at 1370 cm^{-1}.[18]

Figure 3a compares the Raman spectra of the droplets at various WSR and the spectrum of bulk water. For the dilute droplets of WSR = 13.6, four bands at 1049 (ν_1), ~1355 (ν_{3a}), ~1415 (ν_{3b}), and ~720 cm^{-1} (ν_4) were observed. The ν_2 band is Raman forbidden and was not observed. As the WSR decreases, there is little change in the appearance of the bending band (ν_4). However, the symmetric stretching band (ν_1) shifts from 1049 to 1055 cm^{-1} when the WSR decreases from 6.8 to 5.2. This shift is shown clearly in the high-resolution spectra in Figure 3b when the WSR decreases from 7.3 to 5.5. Moreover, a weak shoulder on the higher wavenumber side of the ν_1 band is resolved at about 1060 cm^{-1} when the WSR further decreases to 2.2. The splitting of the two antisymmetric stretching bands (ν_{3a} and ν_{3b}) increases with decreasing WSR, from 60 cm^{-1} (the difference between 1355 and 1415 cm^{-1}) at WSR = 13.6 to 90 cm^{-1} (between 1355 and 1445 cm^{-1}) at WSR = 3.3 (Figure 3a).

Magnesium is an alkali earth metal element in the third period. Having a large charge-to-radius ratio of 3.3 and a high hydration energy,[19] Mg^{2+} has a strong tendency to retain its hexahydrated structure. The hydrated ions of $Mg(H_2O)_6^{2+}$ are therefore very stable. Our previous Raman studies of $MgSO_4$ droplets show that the $\nu_1(SO_4^{2-})$ band shifts from 981 to 1007 cm^{-1} and its full width at half-height (fwhh) increases from 12 to 54 cm^{-1}, when the WSR is reduced from 17.29 to 1.54.[11,12] However, most of the changes do not occur at the saturation WSR of 15.6. Instead, they occur at WSR below 6, where a large number of contact ion pairs including monodentates and bidentates are formed. Similar to $MgSO_4$, $Mg(NO_3)_2$ shows abrupt spectral changes at WSR less than 6. The shift of ν_1 from 1049 to 1055 cm^{-1} is an indicator of the formation of direct contact ion pairs between Mg^{2+} and NO_3^-; i.e., nitrate penetrates the first solvation shell when there are not sufficient water molecules to retain the hexahydrated structure of Mg^{2+}.

The formation of solvent-separated ion pairs and contact ion pairs distorts the symmetry of nitrate ions. This profoundly changes the vibration bands of nitrate in bulk aqueous solutions. For example, the ν_4 mode at 717 cm^{-1} has a new shoulder at about 737−740 cm^{-1} in very concentrated solutions (>7 mol L^{-1}) of $LiNO_3$, due to the formation of contact ion pairs between Li^+ and NO_3^-.[20] The ν_1 band shifts from 1048.5 to 1054 cm^{-1} when the concentration increases from 0.202 to 9.02 mol L^{-1}.[20,21] The Raman spectra of aqueous $Zn(NO_3)_2$ at high pressure and high temperature have a shoulder on the lower wavenumber side of the ν_1 band.[22] Tang et al. found a peak at 812 cm^{-1} (ν_2), which is Raman forbidden in bulk solutions, in supersaturated $Sr(NO_3)_2$ metastable droplets.[23] The ν_1 bands of amorphous $Sr(NO_3)_2$ and $Ca(NO_3)_2$ particles have a much wider fwhh than their solid anhydrous particles.[23]

In $Mg(NO_3)_2$ solutions, contact ion pairs do not exist at concentrations below 3.85 mol L^{-1}.[24] However, they exist at higher concentrations. For example, Peleg[25] measured the Raman spectra of aqueous $Mg(NO_3)_2$ solutions at temperatures between 90 and 120 °C and found that most spectral changes occurred at WSR less than 6. In particular, a blue shift of the ν_1 band from 1049 to 1053 cm^{-1} was observed when the WSR decreased from 6 to 4.2.[25] Peleg explained the shift as nitrate overcoming the polarization effects to form direct contact ion pairs of monodentates with Mg^{2+}. Two new bands at 1034 and 1060 cm^{-1}, which were not observed in solutions or in the melt anhydrous salt, appeared in the $Mg(NO_3)_2 \cdot 2.4H_2O$ melt. They then shifted to 1038 and 1066 cm^{-1} in the $Mg(NO_3)_2 \cdot 2H_2O$ melt. These two bands were attributed to a perturbed quasi-lattice structure of $Mg^{2+}-NO_3^-$ contact ion pairs, even though the detailed structures of the lattice were not reported.

The sudden shift of ν_1 from 1049 to 1055 cm^{-1} at WSR = 6 in Figure 3 coincides with the existence of the transition point of the hydroscopic curve observed in Figure 2. They are both in agreement with the observation of the melt salt reported by Peleg and are attributed to the formation of contact ion pairs with monodentate structures at WSR of 6. A similar association of the change of the hygroscopic property with the formation of contact ion pairs has been reported for some sulfate salts.[11,12] A further decrease in WSR of the droplet did not result in the disappearance of the band at 1053 cm^{-1} and the formation of the two new bands at 1034 and 1060 cm^{-1}, as observed in the hydrate melts ($Mg(NO_3)_2 \cdot 2.4H_2O$). Instead, only a shoulder near 1060 cm^{-1} appeared, which may be related to more complex structures such as bidentates with a composition of ($[Mg^{2+}(H_2O)_{6-2x}(NO_3^-)_x]$, $x = 1-3$) or monodentates with different WSR ($[Mg^{2+}(H_2O)_{6-x}(NO_3^-)_x]$, $x = 1-6$). We will discuss them in the next section. The increase in the separation of the ν_3 bands is also a characteristic of the formation of the complex contact ion pairs.[24,25]

When a droplet was exposed to dry air (RH = 3%) for 10 h, an amorphous particle with WSR of about 2 was occasionally formed. The Raman spectrum of the amorphous particle is shown at the bottom of Figure 3. The ν_1 band appears at 1046 cm^{-1}, with two shoulders at 1035 and 1061 cm^{-1}. In the bending

vibration mode region, two weak peaks are resolved at ~673 and ~723 cm^{-1}. The bands at 1362 and 1422 cm^{-1} are related to the antisymmetric vibration modes. However, no peak was resolved at 830 cm^{-1} (ν_2), which is no longer Raman forbidden and has been observed in amorphous $Sr(NO_3)_2$ particles by Tang et al.[23] All of the peaks of nitrate ions in the amorphous particle show a narrow fwhh, which is a characteristic of freezing nitrate ions and an indication of nitrate ions existing with fixed orientations in microenvironments.

3. Water Structures in $Mg(NO_3)_2$ Droplets. In Figure 3a, the O−H stretching bands of the droplets are very different from the envelope of pure water, which is generally fitted by four components, an ice-like component (C_1) at ~3230 cm^{-1}, an ice-like liquid component (C_2) at ~3420 cm^{-1}, a liquidlike amorphous phase (C_3) at ~3540 cm^{-1}, and monomeric H_2O (C_4) at 3620 cm^{-1}.[13] A main peak always appears at ~3463 cm^{-1} (C_2) when the WSR decreases from 13.6 to 3.0. There is a shoulder at 3269 cm^{-1} (C_1) on the lower wavenumber side of the main peak. Although the wide O−H stretching band is complicated by the regular minor peaks due to Mie morphology resonances, the shape of the envelope of the O−H stretching band is independent of the WSR. After normalization with the main peak at 3463 cm^{-1}, the two spectra of WSR = 13.6 and of WSR = 3.0 are identical (not shown). In fact, the intensity ratio of I_{3269}/I_{3463} is constant from WSR = 3.0 to 13.6. These results suggest that there is little concentration dependence of the hydrogen bonding structures of water on the WSR. The water molecules in the amorphous particles show much more complex features with the four peaks at 3259, 3395, 3497, and 3581 cm^{-1}, corresponding to the four types of water molecules including water monomers.[13]

The hydration parameters of Mg^{2+} ions, e.g., the primary hydration number and the distance of Mg−O $(H_2O)_6$, are not sensitive to the counteranion.[26] X-ray studies of $Mg(NO_3)_2$ solutions have revealed that Mg^{2+} ions have an inner hydration shell of six water molecules and a second coordination shell of twelve water molecules.[26] In this study, the average number of coordinated oxygen atoms per Mg^{2+} is not enough to retain the second layer of Mg^{2+} even for the diluted droplet of WSR = 13.6. Therefore, solvent-separated ion pairs ($[Mg^{2+}(H_2O)_6](H_2O)_{12-y}(NO_3^-)_2$, $y < 4.4$) and direct contact ion pairs of various monodentate ($[Mg^{2+}(H_2O)_{6-x}(NO_3^-)_x]$) and bidentate ($[Mg^{2+}(H_2O)_{6-2x}(NO_3^-)_x]$) structures are found, as illustrated in the Raman spectra shown in Figure 3a. On the basis of Figure 3a, it can be concluded that the water structures in these components have similar hydrogen bonding properties.

4. Raman Image of the Supersaturated Droplets. Figure 4a shows the contour of the Raman image of a diluted droplet with WSR = 9.6. The *x*-axis and the *y*-axis correspond to the Raman shift and the position in the particle along the path of the incident light, respectively. The Raman intensity is represented by colors. The two areas of maximum intensities (red) are the result of the enhanced light scattering at the top and the bottom of the droplet. It is clear that there is a symmetry of the Raman image at $x = 1049$ cm^{-1}, the peak of the Raman spectra at any given position in the droplet. Although the scattering intensities near the edges of the droplets are larger than those at the center, there is no change in the band envelope (i.e., there is a constant peak location) of the spectra at any position after normalization. Thus, the structure of nitrate ions is the same anywhere in the droplet and hence the droplet can be considered homogeneous.

In contrast to a diluted droplet, a supersaturated droplet at WSR= 2.8 is not structurally homogeneous, as evidenced by the Raman image in Figure 4b. Maximum intensities are found near the edges of the droplet. However, the $\nu_1(NO_3^-)$ band shifts to a higher wavenumber near the surface. Three regions can be roughly mapped according to the extent of the band shifts. In the core region, the $\nu_1(NO_3^-)$ peak appears at 1055 cm^{-1} and is symmetric. The intermediate region is characterized by a decrease in the intensity gradient on the lower wavenumber side toward the center of the droplet, indicating the presence of a shoulder at 1039 cm^{-1}. The outer region shows a shift of the $\nu_1(NO_3^-)$ band from 1055 to 1060 cm^{-1} when approaching the surface of the droplet.

Irish et al. have resolved two peaks at 1039 and 1064 cm^{-1} in the hydrate melt of WSR = 2.2.[20] These peaks are related to different bidentate structures of the contact ion pairs $[Mg^{2+}(H_2O)_{6-2x}(NO_3^-)_x]$ between NO_3^- and Mg^{2+}. They proposed that the 1038 and 1060 cm^{-1} peaks correspond to the tetrahydrate bidentate ($[Mg^{2+}(H_2O)_4(NO_3^-)]$) and the dihydrate bidentate ($[Mg^{2+}(H_2O)_2(NO_3^-)_2]$), respectively.[24] The positional dependence of the $\nu_1(NO_3^-)$ characteristic shown in Figure 4b indicates that the supersaturated droplet is structurally heterogeneous.

To understand the relationship between the ν_1 band and the structures of the contact ion pairs between Mg^{2+} and NO_3^-, we used the ab initio method to optimize the configurations of the monodentate and bidentate contact ion pairs on the RHF level with the 6-311++G basis set.[27] Figure 5 shows the optimized structures of monodentate and bidentate contact ion pairs. All the monodentates ($[Mg^{2+}(H_2O)_{6-x}(NO_3^-)_x]$, $x = 1-6$) are local stationary points as minima with no imaginary frequencies. For the bidentates ($[Mg^{2+}(H_2O)_{6-2x}(NO_3^-)_x]$, $x = 1-3$), the tetrahydrate bidentate and the anhydrate bidentate are the local minima. No stable structure was optimized for the dihydrate bidentate because three imaginary frequencies can exist. The calculated frequencies of the ν_1 band of the stable structures as well as their Raman activities are also shown in Figure 5. The calculated vibration frequencies depend on the calculation method and the basis set. The relative position of each vibration mode of NO_3^-, with the calculated frequency of free NO_3^- as a reference, provides an insight of the band shift in the hydration of NO_3^- and the formation of contact ion pairs of NO_3^- with cations. Kelley et al. have performed theoretical analyses on the separation of the degenerate band pairs (the difference between ν_{3a} and ν_{3b}) for nitrate−water complexes at the ab initio Hartree−Fock level with the consideration of diffuse and polarization functions.[18] In our calculations, all the monodentates have calculated frequencies higher than the calculated ν_1 of free NO_3^- ions (1094.3 cm^{-1}) whereas the bidentate contact ion pairs have calculated frequencies lower than that of free NO_3^- ions.

At WSR = 2.8, it is unlikely that free NO_3^- or solvent-separated ion pairs exist with so little water in the droplets. Thus, Figure 4b can be viewed as an indication of the spatial distribution of various contact ion pairs. The core region has a symmetric band at 1055 cm^{-1} and predominantly contains monodentate contact ion pairs of $[Mg^{2+}(H_2O)_5(NO_3^-)]$, supported by the result that the calculated frequency of $[Mg^{2+}(H_2O)_5(NO_3^-)]$ is 1114.9 cm^{-1}, higher than that of free NO_3^- at 1094.3 cm^{-1}.

The intermediate region has the main peak at about 1055 cm^{-1} with a shoulder at ~1039 cm^{-1}. According to the calculated frequencies, we propose that the tetrahydrate bidentate ($[Mg^{2+}(H_2O)_4(NO_3^-)]$) (1038.0 cm^{-1}) exists in the intermediate region even though the main component is still $[Mg^{2+}(H_2O)_5$-

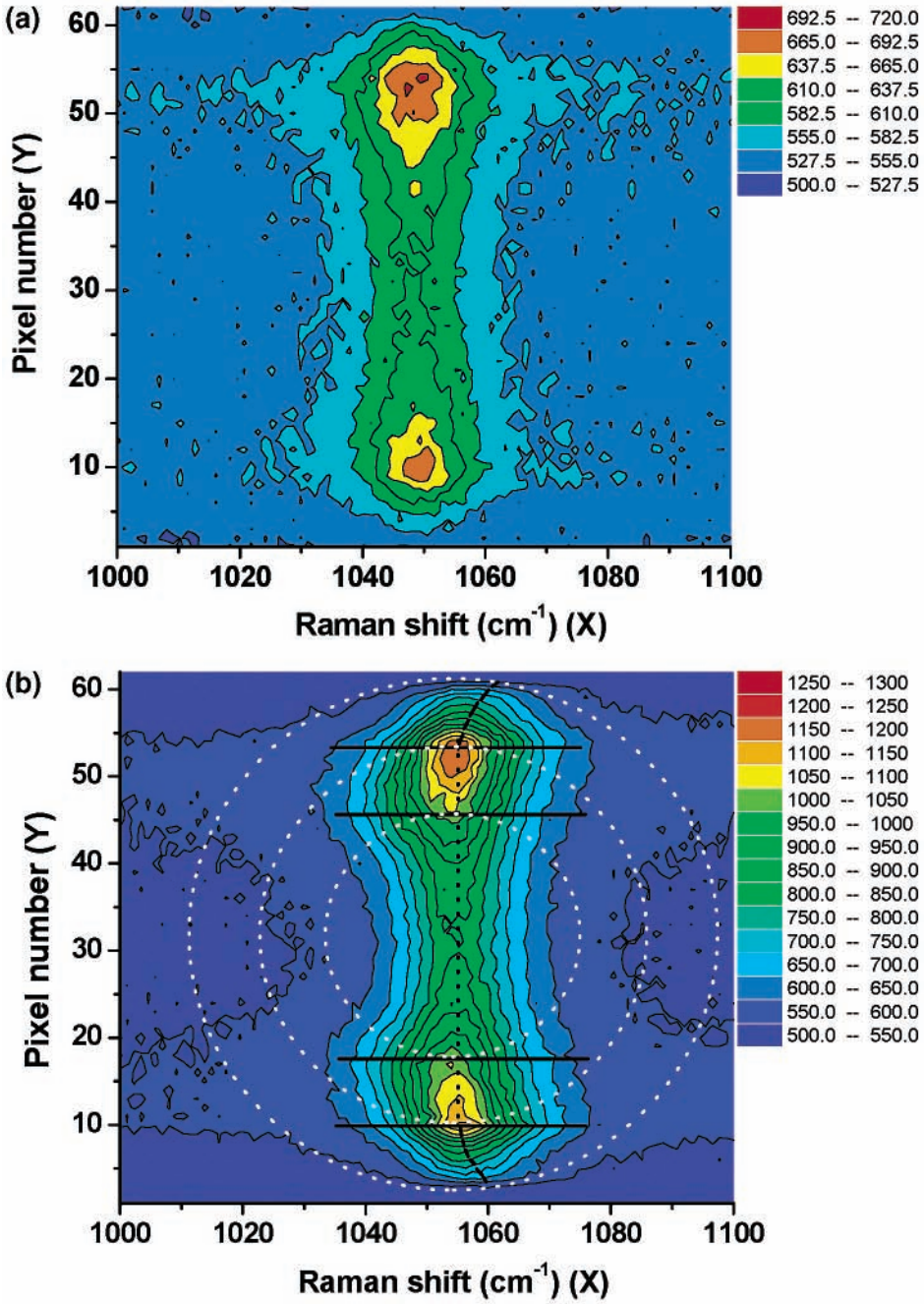

Figure 4. (a) Spatially resolved Raman contours of a dilute $Mg(NO_3)_2$ droplet equilibrated at RH = 70.1% (molar solute-to-water ratio = 9.6). The *x*-axis and *y*-axis correspond to the Raman shift and the position along the vertical axis of the particle, respectively. (b) Spatially resolved Raman contours of a supersaturated $Mg(NO_3)_2$ droplet equilibrated at RH = 2.7% (molar solute-to-water ratio = 2.8).

(NO_3^-)]. Because the overall NO_3^- to Mg^{2+} ratio of the droplet is 2 and the core region has a ratio close to unity, the nitrate deficit must be compensated in the outer regions. Thus we attribute the main peak at 1060 cm^{-1} to the monodentates of ($[Mg^{2+}(H_2O)_{6-x}(NO_3^-)_x]$, $x = 3-6$), of which the calculated frequencies with maximum Raman activity are all higher than that of $[Mg^{2+}(H_2O)_5(NO_3^-)]$. To maintain the hexacoordinated structure of Mg^{2+}, the increase of the NO_3^- to Mg^{2+} ratio will be accompanied by the decrease of the H_2O to Mg^{2+} ratio as the surface of the droplet is approached.

Conclusions

Combining the use of an EDB and Raman spectroscopy, we have shown that the hexacoordination structure of Mg^{2+} has a profound effect on the molecular structures and the hygroscopic properties of $Mg(NO_3)_2$ solutions. The formation of contact ion pairs at WSR = 6 has resulted in significant changes in the Raman spectra of the ν_1 nitrate peak and a transition of the measured hygroscopicity. These observations are consistent with our earlier work on sulfates of Mg^{2+} and other metal ions. Furthermore, the formation of high NO_3^-/Mg^{2+} ratio contact ion pairs can be a plausible explanation of the absence of efflorescence in the evaporation of $Mg(NO_3)_2$ droplets. In this paper, we have advanced our single particle Raman spectroscopic analysis to study the structural heterogeneity of droplets. Our Raman imagining analysis has qualitatively suggested that the NO_3^- to Mg^{2+} ratio of the contact ion pairs increases but the H_2O to Mg^{2+} ratio decreases as the surface of a highly supersaturated droplet is approached. Recently, preferential surface enrichments of anions near droplet surfaces have been

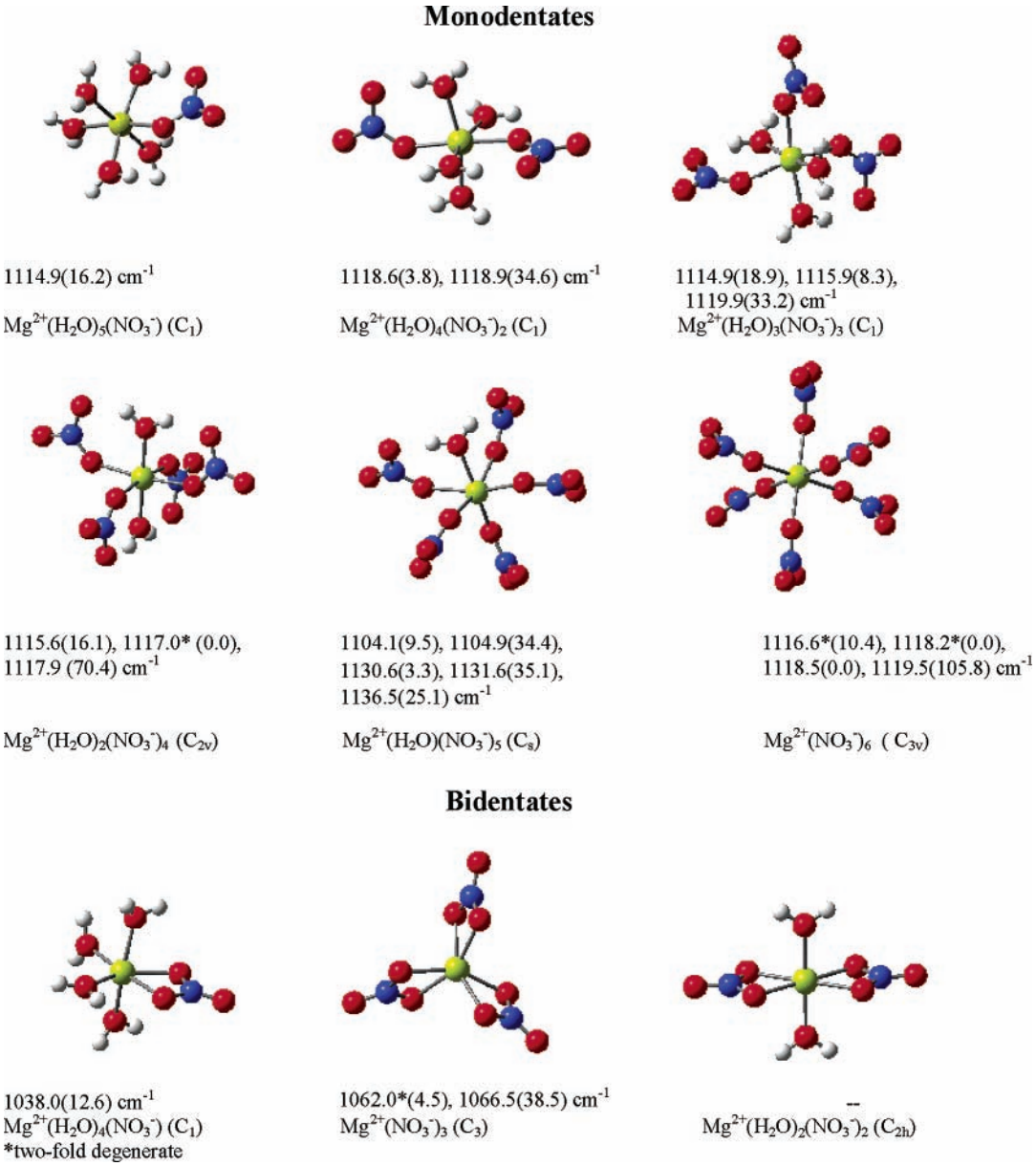

Figure 5. Optimized structures (RHF/6311++G) of the monodentate ($[Mg^{2+}(H_2O)_{6-x}(NO_3^-)_x]$, $x = 1-6$) and the bidentate ($[Mg^{2+}(H_2O)_{6-2x}(NO_3^-)_x]$, $x = 1-3$) contact ion pairs, their calculated frequencies (cm^{-1}) and Raman activities (in parentheses) of the ν_1 bands: (red ball) oxygen atom; (blue ball) nitrogen atom; (yellow ball) magnesium atom; (white ball) hydrogen atom.

associated with the enhanced role of sea-salt aerosols in gas-phase atmospheric chemistry.[28−30] According to the Raman characteristics of contact ion pairs, the "surface enrichment" of contact ion pairs of high NO_3^- to Mg^{2+} ratio only exists in supersaturated droplets. Although this work may not be directly relevant to surface enrichment of anions, which potentially exist even in diluted droplets, it provides experimental evidence to the observation of heterogeneity of droplets. Our laboratory is currently exploring the use of fluorescence spectroscopy to study the surface enhancement of anions of levitated droplets at low concentrations to supersaturation.[31]

Acknowledgment. Financial support from the Hong Kong RGC Earmarked Grant (HKUST6042/01P), the HKUST PDF grant, the National Natural Science Foundation of China (No.20073004) and Trans-Century Training Program Foundation for the Talents of Humanities and Social Science by the State Education Commission is gratefully acknowledged.

References and Notes

(1) Wrinkler, P. *Phys. Scripta* **1988**, 37, 223.
(2) Cohen, M. D.; Flagan, R. C.; Seinfeld, J. H. *J. Phys. Chem.* **1987**, *91*, 4563.
(3) Chan, C. K.; Flagan, R. C.; Seinfeld, J. H. *Atmos. Environ.* **1992**.
(4) Tang, I. N.; Munkelwitz, H. R. *J. Geophys. Res.* **1994**, *99* (D9), 18801.
(5) McMurry, P. H.; Litchy, M.; Huang, P. F.; Cai, X.; Turpin, B. J.; Dick, W. D.; Hanson, A. *Atmos. Environ.* **1996**, *30*, 101.
(6) Hameri, K.; Vakeva, M.; Hansson, H.-C.; Laaksonen, A. *J. Geophys. Res.* **2000**, *105* (D17), 22231.
(7) Cruz, C. N.; Pandis, S. N. *Environ. Sci. Technol.* **2000**, *34*, 4313.
(8) Han, J. H.; Martin, S. T. *J. Geophys. Res.* **1999**, *104* (D3), 3543.
(9) Cziczo, D. J.; Abbatt, J. P. D. *J. Geophys. Res.*, **1999**, *104*, 13781.
(10) Onasch, T. B.; Siefert, R. L.; Brooks, S. D.; Prenni, A. J.; Murray, B.; Wilson, M. A.; Tolbert, M. A. *J. Geophys. Res.* **1999**, *104*, 21317.
(11) Zhang, Y.-H.; Chan, C. K. *J. Phys. Chem. A* **2000**, *104*, 9191.
(12) Zhang, Y.-H.; Chan, C. K. *J. Phys. Chem. A* **2002**, *106*, 285.
(13) Zhang, Y.-H.; Chan, C. K. *J. Phys. Chem. A* **2003**, *107*, 5956
(14) Ha, Z.; Chan, C. K. *Aero. Sci. Technol.* **1999**, *31*, 154
(15) Ahlijah, G. E. B. Y.; Mooney, E. F. *Spectrochim. Acta A* **1969**, *25*, 619.

(16) Bulmer, J. T.; Chang, T. G.; Gleeson, P. J.; Irish, D. E. *J. Solution Chem.* **1975**, *4*, 969.
(17) Irish, D. E.; Davis, D. L. *Can. J. Chem.* **1968**, *46*, 943.
(18) Waterland, M. R.; Stockwell, D.; Kelley, A. M. *J. Chem. Phys.* **2001**, *114*, 6249.
(19) Phillips, C. G.; Williams, R. J. P. *Inorganic Chemistry*; Clarendon Press: NewYork, 1965; Vol. 1, p 161
(20) Irish, D. E.; Nelson, D. L.; Brooker, M. H. *J. Chem. Phys.* **1971**, *54*, 654.
(21) Tomisici, V.; Simeon, V. *Phys. Chem. Chem. Phys.* **2000**, *2*, 1943].
(22) Ikushima, Y.; Satio, N.; Arai, M. *J. Phys. Chem. B* **1998**, *102*, 3029.
(23) Tang, I. N.; Fung, K. H. *J. Chem. Phys.* **1997**, *106*, 1653.
(24) Chang, T. G.; Irish, D. E. *J. Phys. Chem.* **1973**, *77*, 52.
(25) Peleg, M. *J. Phys. Chem.* **1972**, *76*, 1019.
(26) Caminiti, R.; Licheri, G.; Picaluga, G.; Pinna, G. *Chem. Phys. Lett.* **1979**, *61*, 45.
(27) Frisch, M. J.; Trucks, G. W.; Schlegel, H. B.; Scuseria, G. E.; Robb, M. A.; Cheeseman, J. R.; Zarzewski, V. G.; Montgomery, J. A., Jr.; Stratman, R. E.; Burant, J. C.; Dapprich, S.; Millam, J. M.; Daniels, A. D.; Kudin, K. N.; Strain, M. C.; Farkas, O.; Tomasi, J.; Barone, V.; Cossi, M.; Cammi, R.; Mennucci, B.; Pomelli, C.; Adamo C.; Clifford, S.; Ochterski, J.; Peterson, J. A.; Ayala, P. Y.; Cui, Q.; Morokuma, K.; Malick, D. K.; Rabuck, A. D.; Ragvachakari, K.; Foresman, J. B.; Cioslowski, J.; Ortiz, J. V.; Baboul, A. G.; Stefanov, B. B.; Liu, G.; Liashenko, A.; Piskorz, P.; Komaromi, I.; Gomperts, R.; Martin, R. L.; Fox, D. J.; Keith, T.; Al-Laham, M. A.; Peng, C. Y.; Nanayakkare, A.; Challacombe, M.; Gill, P. M. W.; Johnson, B.; Chen, W.; Wong, M. W.; Andres, J. L.; Gonzales, C.; Head-Gordon, M.; Replodge, R. S.; Pople, J. A. Gaussian98, revision A9; Gaussian; Inc.: Pittsburgh, PA, 1998.
(28) Seinfeld, J. H. *Science* **2000**, *288*, 285.
(29) Jungwirth, P. *J. Phys. Chem. A* **2000**, *104*, 145.
(30) Knipping, E. M.; Lakin, M. J.; Foster, K. L.; Jungwirth, P.; Tobias, D. J.; Gerber, R. B.; Dabdub, D.; Finlayson-Pitts, B. J. *Science* **2000**, *288*, 301.
(31) Choi M. Y.; Chan, C. K.; Zhang Y. H. *J. Phys Chem A*, 2004, *108*, 1133.